Artvin Çoruh Üniversitesi
Doğal Afetler Uygulama ve Araştırma Merkezi
Doğal Afetler ve Çevre Dergisi

Artvin Çoruh University
Natural Hazards Application and Research Center
Journal of Natural Hazards and Environment

Araştırma Makalesi / Research Article, Doğ Afet Çev Derg, 2024; 10(2): 295-313, DOI: 10.21324/dacd.1407354

Flood risk assessment using Neutrosophic Analytical Hierarchy Process (N-AHP) and GIS techniques in the Melet Basin (Türkiye)

Murat Fıçıcı[1,*]

[1]*Ardahan University, Faculty of Humanities and Letters, Department of Geography, 75000, Ardahan, Türkiye.*

Abstract

Today, knowing the spatial distribution of flood risk using GIS (Geographic Information Systems)-based MCDM (Multi-Criteria Decision Making) approaches has been a topic addressed by many researchers. In this context, the current study focuses on the spatial distribution of flood risk using the N-AHP (Neutrosophic Analytical Hierarchy Process)-based GIS approach. The Melet Basin (Türkiye) is a case study for the suggested methodology. Four decision-makers used linguistic phrases to compare and assess the flood criteria during the method's application phase. The opinions of the decision makers were combined with the N-AHP, and the criteria were weighted. The results determined that precipitation, distance from the river, drainage density, land use, and slope were the most important factors affecting the flood and contributed approximately 74%. Apart from this, it has been observed that 10% of the basin is in the high and very high flood risk classes, and these risky areas overlap with the flood points of past periods. The proposed approach and findings are anticipated to have theoretical and practical implications.

Keywords

Neutrosophic Set, MCDM-GIS, AHP, Flood Risk, Melet Basin, Türkiye

Nötrosofik Analitik Hiyerarşi Süreci (N-AHS) ve CBS Teknikleri Kullanılarak Melet Havzası'nda (Türkiye) Taşkın Risk Değerlendirmesi

Özet

Günümüzde CBS (Coğrafi Bilgi Sistemleri) tabanlı ÇKKV (Çok Kriterli Karar Verme) yaklaşımları kullanılarak taşkın riskinin mekansal dağılımının bilinmesi birçok araştırmacının ele aldığı bir konu olmuştur. Bu bağlamda mevcut çalışma, N-AHS (Nötrosofik Analitik Hiyerarşi Süreci) tabanlı CBS yaklaşımını kullanarak taşkın riskinin mekansal dağılımına odaklanmaktadır. Önerilen yaklaşım Melet Havzası'nda (Türkiye) bir örnek olay olarak incelenmiştir. Yöntemin uygulama aşamasında dört karar verici taşkın kriterlerini dilsel terimler kullanarak birbirleriyle karşılaştırmıştır. Karar vericilerin görüşleri N-AHS ile birleştirilerek kriterler ağırlıklandırılmıştır. Sonuçlar, yağış, nehirden uzaklık, drenaj yoğunluğu, arazi kullanımı ve eğimin taşkını etkileyen en önemli faktörler olduğunu ve bu faktörlerin yaklaşık %74 oranında taşkına neden olduğu belirlenmiştir. Bunun dışında havzanın %10'unun yüksek ve çok yüksek taşkın riski sınıflarında yer aldığı ve bu riskli alanların geçmiş dönemlerin taşkın noktalarıyla örtüştüğü görülmüştür. Önerilen yaklaşım ve bulguların teorik ve pratik çıkarımlara sahip olması beklenmektedir.

Anahtar Sözcükler

Nötrosofik Küme, ÇKVV-GIS, AHS, Taşkın Riski, Melet Havzası, Türkiye

1. Introduction

Flooding is a disaster often associated with natural and anthropogenic conditions, causing flooding of land or rivers (Mishra & Sinha, 2020). Flood events are considered one of the most dangerous and widespread natural disasters due to their devastating effects on many people and the natural environment worldwide (Foudi et al., 2015; Li et al., 2016; Mudashiru et al., 2022b). Because highly complex and dynamic processes play a role in floods' formation, preventing their occurrence is almost impossible (Pappenberger et al., 2006; Wu et al., 2022). Therefore, to analyse floods effectively, it is necessary to know the degree of impact of flood factors based on the characteristics of the basins (Mudashiru et al., 2022a). Flood risk assessment has become one of the hottest topics in natural sciences and technology worldwide. Numerous techniques have been put forth and used recently for mapping flood risk. In particular, GIS and remote sensing methods were focused on to evaluate the flood risk from a topographic, meteorological and socioeconomic perspective (Cai et al., 2019; Özşahin, 2022). The methods above have allowed for the regional assessment of flood hazard zones, often along the axis of different variables influencing the development of this natural disaster (Lappas & Kallioras, 2019; Liu et al., 2019; Wu et al., 2022). Several factors influence and increase flood risk, including hydrology, population, poor land use, inadequate drainage systems, and geoenvironmental features (Mudashiru et al., 2022a; Zhang et al, 2018).

* Corresponding Author: Tel: +90 (478) 2117575 Fax: +90 (478) 2117527
E-mail: muratficici@ardahan.edu.tr (Fıçıcı M)
Gönderim Tarihi / Received : 20/12/2023
Kabul Tarihi / Accepted : 24/03/2024

While the mentioned factors usually consist of qualitative factors with different layers and complex structures, determining the impact of these factors plays a crucial role in flood assessment (Wu et al., 2022). Many studies have applied GIS-based MCDA (Multi-Criteria Decision Analysis) for flood risk assessment in this context (Jun et al., 2013; Chen et al., 2015; Arabameri et al., 2019; Hammami et al., 2019; Toosi et al., 2019; Kanani-Sadat et al., 2019; Mishra & Sinha, 2020; Aydın & Birincioğlu, 2022; Taş & Yanık, 2022). The most commonly used MCDM technique was AHP (Analytical Hierarchy Process). AHP is an MCDM technique that allows determining the priority and weight values of the factors that are effective in decision-making in a problem. AHP offers a practical approach to quantify the parameters affecting the flood, especially in flood risk mapping. However, AHP does not consider the inconsistency or bias of decision-makers in pairwise comparison. This may lead to doubts and uncertainties in the assessment of flood risk (Wu et al., 2022). Against this limitation of the AHP technique, many researchers have suggested the use of Zadeh (1965)'s fuzzy set (FS) theory with AHP (Abdel Basset et al., 2018a; Vafadarnikjoo & Scherz, 2021; Yucesan & Gul, 2021). To capture uncertainty, several flood assessment studies have concentrated on the fuzzy AHP (F-AHP), an extension of the AHP based on fuzzy sets (FS). The fuzzy set, on the other hand, is limited to the membership function. It has failed to capture the ambiguity in the real world because it ignores non-membership and uncertainty (Abdel-Basset et al., 2018a; 2018b). Because of this, Smarandache (1995) developed the notion of neutrosophic sets (NS), in which information is represented by three membership degrees that are ambiguous and inconsistent. Membership degrees in NS consist of three independent membership functions called truth-membership $T_A(x)$, falsity-membership $F_A(x)$, and uncertainty-membership $I_A(x)$ functions (Stanujkić et al., 2021). Later, Wang et al. (2010) proposed a different version of NS, the single valued neutrosophic set (SVNS). Recently, many researchers have focused on NSs, SVNSs and their extensions to solve complex MCDM problems that are inherently uncertain and inconsistent. In the literature, many studies (Ahmad & Simonovic, 2011; Yang et al., 2013; Lai et al., 2015; Hategekimana et al., 2018; Lyu et al., 2020; Tella & Balogun, 2020; Ekmekçioğlu et al., 2021; Vilasan & Kapse, 2021; Cai et al., 2021; Souissi et al., 2022; Arca & Yalçın, 2023 e.g.) evaluate flood risk with fuzzy sets. However, the integrated use of NS and AHP has not been found in the flood risk assessment literature. However, some studies have addressed the extension of AHP simultaneously with Neutrosophic Set (NS) theories, which can improve decision-making in uncertain environments (Abdel-Basset et al., 2018a; 2018b; Vafadarnikjoo et al., 2018; Stanujkić et al., 2021; Vafadarnikjoo et al., 2021; Vafadarnikjoo & Scherz, 2021). It is stated that integrating neutrosophic logic with AHP eliminates the need for consistent data to be obtained by experts (Kaur & Garg, 2022). This will allow more objective results to be brought in flood risk assessment. Due to the advantages of N-AHP and the literature gaps, it aims to use the approach mentioned in the current study in an integrated manner with GIS. For this purpose, the Melet River Basin, one of the important basins of Turkey, was chosen as the study area. Many flood disasters have occurred, especially in the lower part of the basin. With changes in land use, the risk of possible floods in the basin continues (Şenol, 2019b). Therefore, the proposed approach was tested in this basin. Testing which factors are more effective in these floods with the proposed approach can provide various insights to explain flood behaviour. In addition, fuzzing the GIS-AHP approach, frequently used in flood studies, will give a more objective and theoretically based contribution to the subject area.

2. Description of the Study Area

The Melet River Basin is located on the eastern border of the Central Black Sea Section of the Black Sea Region. The Melet River is located approximately between latitudes 40° 20' and 40° 59' N and longitudes 37° 36' and 38° 02' E. Bird flight to the Black Sea originates from the vicinity of Karagöl Mountain (3107 m), which is 70 km away, passing through Ordu province and pouring into the Black Sea. The Melet River Basin features a dendritic drainage network with a width of approximately 70 km in north-south and 30 km in east-west directions (Figure 1).

The eastern borders of the Melet River Basin from the Black Sea coastal belt; Bahşışkıranı (423 m), Fındıklı (457 m), Düzyatak (1059 m), Gürgen (1271 m), Aydoğan (1971 m), Kayabaşı (1756 m), Gerişüstü (1708 m) and Körgöz (2030 m) hills form, Its eastern borders are Dikilisırik (2212 m), Çakıl (2108 m), Karagöl (3107 m), Yıldız (1836 m), Summer (2012 m), Koru (2123 m) and Kabadüz (889 m) hills. Dozens of tributaries, such as Sap, Kanlı and Baldıran, are connected to the Melet River. The basin is a profoundly cleaved valley through the Melet River and its tributaries (Figure 1).

The Melet River Basin completed its geological development from the Cretaceous to the Quaternary. Upper Cretaceous aged limestones and Tertiary volcanic are found on the Gerişüstü, Körgöz and Dikilisırık Hills, which form the peaks belt in the south of the basin. Moving south from the summits section, there are Upper Cretaceous aged volcanic around Mesudiye, Upper Cretaceous aged granitoid in Topçam, Upper Cretaceous aged volcanic in Kabadüz, and Quaternary alluviums in the Black Sea coastal belt (Keskin, 2011; Sümengen, 2013). Most of the Melet River Basin comprises volcanic rocks and a small portion of metamorphic rocks (Figure 3).

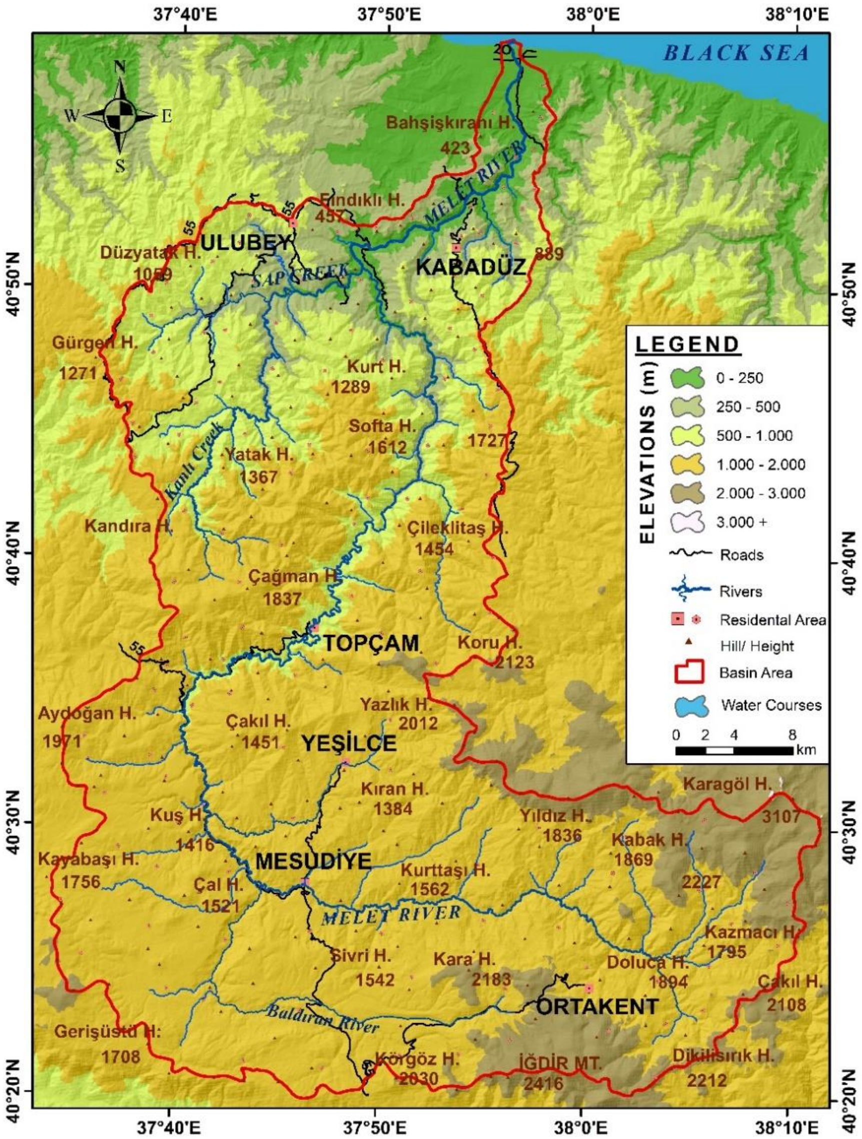

Figure 1: Location map of the Melet River Basin

The Black Sea Region, where the Melet basin is located, has the highest rainfall in Turkey. For this reason, frequent flood events occur in the Black Sea coastal belt rivers. Various flood events have occurred in the Melet basin in the past years. In the Melet Basin, nearly 20 flood events occurred from 1944 to 2014 (Hatipoğlu, 2017). With the opening of the river beds in the basin for settlement, any loss of life and property may occur in the floods (Şenol, 2019a). This is among the most important problems of Turkey and the basin waiting to be solved.

3. Methodology

The GIS multi-criteria decision analysis (MCDA) structure is used in the study's methodology. In this approach, flood risk analysis of the Melet River Basin in the Black Sea Region of Turkey was carried out using GIS and NS-AHP. The principles of NS and the application steps of the methodological approach are presented in the following sections.

3.1 Geospatial Data Sources and Preparation

Various parameters need to be determined to evaluate flood susceptibility and create a flood model. Since there is no fixed model in the literature, the use of parameters may vary according to different spatial scales (Tehrany et al., 2014). Eleven factors were used in this study to create appropriate thematic maps. Characteristics of the Melet Basin and previous research (Ghosh & Kar, 2018; Souissi et al., 2022; Tella & Balogun, 2020; Penki et al., 2022; Negese et al., 2022; Mudashiru et al., 2022b) were used to determine the following flood susceptibility factors. The methodological flow of this study is shown in Figure 2. Table 3 presents the data used in the research and their characteristics.

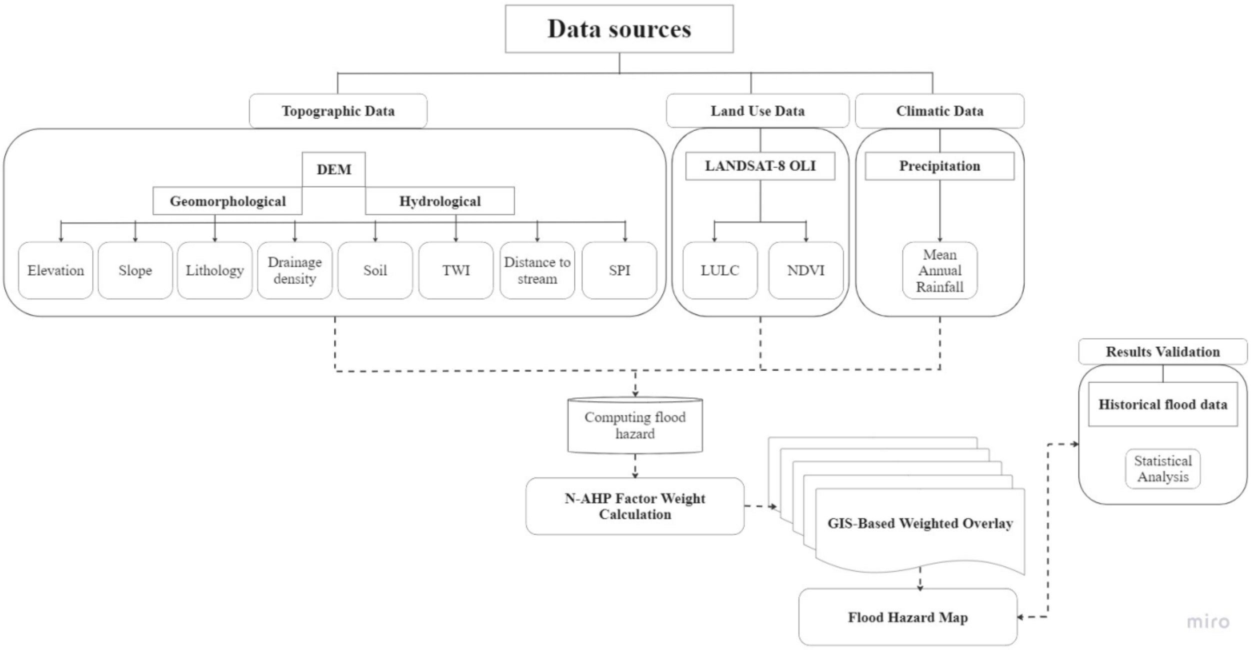

Figure 2: Flow chart

Table 1: Geospatial data and sources

Data	Year	Source	Extracted data
ASTER GDEM	2020	USGS (United States Geological Survey) Earth Explorer	Elevation, slope, TWI, distance to stream, drainage density, SPI
LANDSAT-8 OLI	2019	USGS Earth Explorer	LULC (Land Use and Land Cover)
Digital Soil Map of the District	2018	Map General Command	Soil map
AnnualyRainfall Data	1970-2022	National Weather Station	Rainfall map
Geology	2020	MTA (English- General Directorate of Mineral Research and Exploration)	Lithology map
Flood inventory points	1960-2020	AFAD (English- Disaster and Emergency Management Presidency) and Literature	

While determining the boundaries of the research area, the river branches joining the Melet River were followed. The watershed lines were drawn on 27 maps following the water division lines on the 1/25.000 scale topography maps. All the parameters that create the flood risk have been calculated by considering this limit, and the risky areas have been determined by subjecting the weighted overlap analysis. In creating thematic maps of the research area, firstly, the elevation model of the basin was downloaded using the Digital Elevation Map (DEM) data, the United States Geological Survey (USGS) database, which constitutes the study area. This downloaded data was arranged in the following stages to create a primary data source for the TWI, SPI, slope analysis and elevation parameters. DEM data are up-to-date data of 2022 for satellite bands n40_e37 and n40_e38 via ASTER GDEM.

The DEM data of the research area was cut in accordance with the field boundaries. Before this stage, since the data covering the study area consisted of two separate bands, the collection process was carried out under a single band. Arc Toolbox Data Management Tools Raster Dataset Mosaic to New Raster operations on ArcGIS 10.8 created a single band out of the data, which was then extracted using the Extract by Mask method and clipped according to the field. The cut data is manually divided into five classes with Spatial Analyst Tools→Reclass→Reclassify operation.

Slope analysis used in flood risk analysis was created by applying Arc Toolbox→Spatial Analyst Tools→Surface→Slope analysis using DEM data as baseline data. The slope parameter created was divided into six classes again according to the slope classes in the literature, and a weight value was assigned to each of them.

The data related to the amount of precipitation, another parameter, was created in an Excel environment of 52 years of precipitation data on a monthly basis, taking the averages in parallel with the altitude. Here, Schreiber's 54 mm precipitation increase in every 100 m was applied to the research area, and then the precipitation data were evaluated in 5 different classes and weight coefficients were assigned. The precipitation data set, arranged according to Schreiber, was adapted according to the formula below;

$$P_h = P_o + (54 * h) \quad (1)$$

The distance to the river's parameter used in the flood risk analysis is processed with the Analysis Tools → Proximity → Multiple Ring Buffer analysis via ArcGIS over the previously created river lines about the distance to the river lines, and the value increases as the buffer moves away from the rivers at the closest distance with the highest weight value. It was formed by giving the values where the state of the Here, again, the classification was made and the weighting process was carried out so that the weight values were suitable for the classes.

In the study of bedrock (lithology) parameters, manual digitization of MTA 1/100,000 scaled G39-40 and H39-40 sheets on ArcGIS was primarily performed. In the next step, the main rock groups were assigned weight coefficients by adding a separate field as sedimentary, volcanic and metamorphic rocks within themselves. The map was converted to raster format by Arc Toolbox → Conversion Tools → To Raster → Polygon to Raster operation of the leading rock groups forming the basin according to the assigned weight coefficients.

The drainage density parameter was carried out with the Arc Toolbox→Spatial Analyst→Density→Line Density process to determine how long the stream density per unit area after the digitization of the streams from the 1st index forming the basin up to the highest level. After this stage, the densities were reclassified, and the polygon data was created. A new field has been added to the completed new polygon data, and weight coefficients have been entered. The conversion process from polygon to raster data format was performed according to this new data set.

Data with the .shp extension produced by the General Command of Mapping was used to create the factor map for the soil. The soil groups in the data set were separated according to the Large Soil Groups, the field was added, and the weight coefficient definition was made for the new field added. This newly created data set was converted from polygon data to raster format according to weight coefficients.

The land cover and management in the research area were prepared in 2020 using the data of the European Environment Agency CORINE (Coordination of Information on the Environment). By adding a new field to the data set, weighting coefficients were given and converted to raster format.

Topographic Wetness Index and Stream Power Index calculations were calculated from the Flow Accumulation data created using the research area's DEM data as raw data. While making the estimates, operations were carried out on the DEM data used before and Slope analysis over ArcGIS Map Algebra.

$$TWI = \ln\left(\frac{A_s}{\tan\beta}\right) \tag{2}$$

$$SPI = \ln(A_s.\tan\beta) \tag{3}$$

NDVI analysis was performed to determine biological activities on behalf of plant index values (Tucker, 1979). In NDVI analysis, values vary between -1 and +1. Here, negative values reveal lands devoid of vegetation; values between 0.001 and 0.33 indicate maquis, bushes or neglected areas, while values between 0.33 and 0.66 indicate forested lands. Values above 0.66 indicate the presence of dense forest and a lively surface. LANDSAT-8 OLI data was used when conducting the NDVI analysis. Here, the data of bands 4 and 5 are processed. Vegetation status was tried to be determined by applying the data of bands belonging to near-infrared and red colours 2016_01_T1_B4 and 2016_01_T1_B5 bands with Map Algebra on Raster Calculator in ArcGIS environment to the following formula;

$$NDVI = \frac{(NIR - Red)}{(NIR + Red)} \tag{4}$$

3.2 Preliminaries: Neutrosophic Set Theory

The neutrosophic theory was developed by Florentin Smarandache in 1998. On the other hand, SVNS (Single-Valued Neutrosophic Sets), considered a subclass of the neutrosophic set, is, suggested by Wang et al. (2010). This section provides definitions for NS and SVNS.

Definition 1 Neutrosophic set (NS) (Smarandache, 1999; Vafadarnikjoo, 2020). Let X be a point-space (object-space) in A where the generic elements are represented by x. The truth-membership function $T_A(x)$, the uncertainty-membership function $I_A(x)$, and the false-membership function $F_A(x)$ define a neutrosophic set in X, A. The functions TA(x), IA(x), and FA(x) are true standard or nonstandard subsets of]0−, 1+ [. Namely, $T_A(x)$⟶]0− , 1+ [, $I_A(x)$⟶]0− , 1+ [and $F_A(x)$⟶]0− , 1+ [. Therefore, there is no care on the sum of $T_A(x)$, $I_A(x)$ and $F_A(x)$ i.e., $0^- \leq T_A(x) + I_A(x) + F_A(x) \leq 3^+$.

Definition 2 Single-valued neutrosophic set (SVNS) (Wang et al., 2010). Let X be a space of points (objects) with generic elements denoted by x in X. A SVNS A in X is characterized by the truth-membership function $T_A(x)$, the uncertainty-membership function $I_A(x)$ and the false-membership function $F_A(x)$. So a SVNS A can be denoted by $A = \{\langle x, T_A(x), I_A(x), F_A(x)\rangle x \in X\}$, where $T_A(x)$, $I_A(x)$, $F_A(x)$∈ [0, 1] for every x point in X. Therefore, the sum of $T_A(x)$, $I_A(x)$ and $F_A(x)$satisfies the condition $0 \leq T_A(x) + I_A(x) + F_A(x) \leq 3$.

Definition 3 Single-valued trapezoidal neutrosophic number (SVTNN) (Deli & Subas, 2014; Vafadarnikjoo et al., 2021; Vafadarnikjoo & Scherz, 2021). An SVTNN $\tilde{a} = <(a_1, b_1, c_1, d_1); w_{\tilde{a}}, u_{\tilde{a}}, y_{\tilde{a}} >, a_1, b_1, c_1, d_1 \in R, a_1 \le b_1 \le c_1 \le d_1$, and $w_{\tilde{a}}, u_{\tilde{a}}, y_{\tilde{a}} \in [0,1]$ is a particular single-valued neutrosophic number (SVNN) whose $T_{\tilde{a}}(x)$, $I_{\tilde{a}}(x)$ and $F_{\tilde{a}}(x)$ are presented as the following Eqs. (5) to (7) respectively:

$$T_{\tilde{a}}(x) = \begin{cases} \frac{(x-a_1)w_{\tilde{a}}}{(b_1-a_1)}, a_1 \le x < b_1, \\ w_{\tilde{a}}, \quad b_1 \le x \le c_1, \\ \frac{(d_1-x)w_{\tilde{a}}}{(d_1-c_1)}, c_1 < x \le d_1, \\ 0, \quad otherwise, \end{cases} \tag{5}$$

$$I_{\tilde{a}}(x) = \begin{cases} \frac{(b_1 - x + u_{\tilde{a}}(x-a_1))}{(b_1-a_1)}, a_1 \le x < b_1, \\ u_{\tilde{a}}, \quad b_1 \le x \le c_1, \\ \frac{(x - c_1 + u_{\tilde{a}}(d_1-x))}{(d_1-c_1)}, c_1 < x \le d_1, \\ 1, \quad otherwise, \end{cases} \tag{6}$$

$$F_{\tilde{a}}(x) = \begin{cases} \frac{(b_1 - x + y_{\tilde{a}}(x-a_1))}{(b_1-a_1)}, a_1 \le x < b_1, \\ y_{\tilde{a}}, \quad b_1 \le x \le c_1, \\ \frac{(x - c_1 + y_{\tilde{a}}(d_1-x))}{(d_1-c_1)}, c_1 < x \le d_1, \\ 1, \quad otherwise, \end{cases} \tag{7}$$

Definition 4 (Vafadarnikjoo et al., 2021). Let $\tilde{a} = \langle (a_1, b_1, c_1, d_1); w_{\tilde{a}}, u_{\tilde{a}}, y_{\tilde{a}} \rangle$ *and* $\tilde{b} = \langle (a_2, b_2, c_2, d_2); w_{\tilde{b}}, u_{\tilde{b}}, y_{\tilde{b}} \rangle$ be two SVTNNs and $\lambda \ne 0$ and positive then.

$$\begin{aligned} &\tilde{a} + \tilde{b} = \langle (a_1 + a_2, b_1 + b_2, c_1 + c_2, d_1 + d_2); w_{\tilde{a}} + w_{\tilde{b}} - w_{\tilde{a}} w_{\tilde{b}}, u_{\tilde{a}} u_{\tilde{b}}, y_{\tilde{a}} y_{\tilde{b}} \rangle \\ &\tilde{a}\tilde{b} = \langle (a_1 a_2, b_1 b_2, c_1 c_2, d_1 d_2); w_{\tilde{a}} w_{\tilde{b}}, u_{\tilde{a}} + u_{\tilde{b}} - u_{\tilde{a}} u_{\tilde{b}}, y_{\tilde{a}} + y_{\tilde{b}} - y_{\tilde{a}} y_{\tilde{b}} \rangle \\ &\lambda \tilde{a} = \langle (\lambda a_1, \lambda b_1, \lambda c_1, \lambda d_1); 1 - (1 - w_{\tilde{a}})^{\lambda}, u_{\tilde{a}}^{\lambda}, y_{\tilde{a}}^{\lambda} \rangle \\ &\tilde{a}^{\lambda} = \langle (a_1^{\lambda}, b_1^{\lambda}, c_1^{\lambda}, d_1^{\Gamma}); w_{\tilde{a}}^{\lambda} 1 - (1 - u_{\tilde{a}})^{\lambda}, 1 - (1 - y_{\tilde{a}})^{\lambda} \rangle \end{aligned} \tag{8}$$

Definition 5 The TNWAA operator (Ye, 2017; Vafadarnikjoo et al., 2021; Vafadarnikjoo & Scherz, 2021). Let $\tilde{a}_j =< (a_j, b_j, c_j, d_j); w_{\tilde{a}}, u_{\tilde{a}}, y_{\tilde{a}} > (j = 1,2, \dots, n)$ be a set of SVTNNs, then a trapezoidal neutrosophic weighted arithmetic averaging (TNWAA) operator is computed on the based-on Eq. (9):

$$\begin{aligned} &TNWAA(\tilde{a}_1, \tilde{a}_2, \dots, \tilde{a}_n) = \sum_{j=1}^{n} p_j \tilde{a}_j \\ &=< \left(\sum_{j=1}^{n} p_j a_j, \sum_{j=1}^{n} p_j b_j, \sum_{j=1}^{n} p_j c_j, \sum_{j=1}^{n} p_j d_j \right); 1 \\ &\prod_{j=1}^{n} \left(1 - w_{\tilde{a}_j}\right)^{pj}, \prod_{j=1}^{n} u_{\tilde{a}_j}^{pj}, \prod_{j=1}^{n} y_{\tilde{a}_j}^{pj} >, \end{aligned} \tag{9}$$

where p_j is the weight of $\tilde{a}_j (j = 1,2, \dots, n)$ while $p_j > 0$, and $\sum_{j=1}^{n} p_j = 1$.

Definition 6 Scorefunction of a SVTNN (Ye, 2017; Vafadarnikjoo et al., 2021; Vafadarnikjoo & Scherz 2021). Given $\tilde{a} = < (a, b, c, d); w_{\tilde{a}}, u_{\tilde{a}}, y_{\tilde{a}} >$ and $a, b, c, d > 0$. Then, the score function of $\tilde{a}$ can be calculated in accordance with the following Eq. (10):

$$S(\tilde{a}) = \frac{1}{12}(a + b + c + d)(2 + w_{\tilde{a}} - u_{\tilde{a}} - y_{\tilde{a}}), S(\tilde{a}) \in [0,1]. \tag{10}$$

Definition 7 In order to compare two SVTNNs (Vafadarnikjoo and Scherz 2021). $\tilde{a} = < (a_1, b_1, c_1, d_1); w_{\tilde{a}}, u_{\tilde{a}}, y_{\tilde{a}} >$, and $\tilde{b} = < (a_2, b_2, c_2, d_2); w_{\tilde{b}}, u_{\tilde{b}}, y_{\tilde{b}} >$where$a_1, b_1, c_1, d_1, a_2, b_2, c_2, d_2 > 0$,then according to Eq. (7), the score functions will be computed, and if $S(\tilde{a}) > S(\tilde{b})$,then $\tilde{a} > \tilde{b}$; if $S(\tilde{a}) = S(\tilde{b})$, then $\tilde{a} = \tilde{b}$.

3.3 The N-AHP procedure

The steps of the proposed N-AHP method to analyze the weights of the factors affecting the flood risk in the Melet River Basin and to provide a ranking are as follows (Abdel-Basset et al., 2018a; Vafadarnikjoo et al., 2021; Vafadarnikjoo & Scherz, 2021).

Step 1: The problem, which consists of goals and criteria, is structured hierarchically.

Step 2: Pairwise comparisons are made for the criteria. DMs use a linguistic expression on a scale of 1-9 (Saaty, 1980) to determine the importance of each item.

Table 2: The importance rating scale (Saaty, 2005).

Numerical scala	Verbal scale	Abbreviations
1	Equal importance	EI
2	Weak importance	WI
3	Moderate importance	MI
4	Moderate plus importance	MPI
5	Strong importance	SI
6	Strong plus importance	SPI
7	Very strong importance	VSI
8	Very very strong importance	VVSI
9	Extreme importance	EXI

Based on the experts' answers, pairwise comparison matrices (n × n) are arranged using Eq. (11).

$$\tilde{A}_k = [a_{ijk}] = \begin{bmatrix} 1 & a_{12k} & \dots & a_{1nk} \\ 1/a_{12k} & 1 & \dots & a_{2nk} \\ \vdots & \vdots & \ddots & \vdots \\ 1/a_{1nk} & 1/a_{2nk} & \dots & 1 \end{bmatrix} \tag{11}$$

Step 3: The consistency ratio (CR) is calculated; the consistency ratio must be less than 0.1 for all pairwise comparisons.

$$CR = \frac{((\lambda_{max} - n)/(n-1)}{RI} \tag{12}$$

Step 4: Values in the initial pairwise comparison matrices are replaced with SVTNNs using the scale shown in Table 2.

Table 3: Neutrosophic rating scale (Vafadarnikjoo & Scherz, 2021)

Numerical scale	SVTNNs	Score function
1/9	⟨(0.11, 0.11, 0.11, 0.11); 1, 0, 0⟩	0.11
1/8	⟨(0.11, 0.11, 0.13, 0.14); 1, 0, 0⟩	0.12
1/7	⟨(0.11, 0.13, 0.14, 0.17); 1, 0, 0⟩	0.14
1/6	⟨(0.13, 0.14, 0.17, 0.2); 1, 0, 0⟩	0.16
1/5	⟨(0.14, 0.17, 0.2, 0.25); 1, 0, 0⟩	0.19
1/4	⟨(0.17, 0.20, 0.25, 0.33); 1, 0, 0⟩	0.24
1/3	⟨(0.14, 0.17, 0.33, 0.50); 1, 0, 0⟩	0.29
1/2	⟨(0.20, 0.25, 0.5, 1); 1, 0, 0⟩	0.49
1/9	⟨(0.11, 0.11, 0.11, 0.11); 1, 0, 0⟩	0.11
1	⟨(1, 1, 1, 1); 0.5, 0.5, 0.5⟩	0.5
2	⟨(1, 2, 4, 5); 0.4, 0.65, 0.6⟩	1.15
3	⟨(2, 3, 6, 7); 0.3, 0.75, 0.7⟩	1.28
4	⟨(3, 4, 5, 6); 0.6, 0.35, 0.4⟩	2.78
5	⟨(4, 5, 6, 7); 0.8, 0.15, 0.2⟩	4.49
6	⟨(5, 6, 7, 8); 0.7, 0.25, 0.3⟩	4.66
7	⟨(6, 7, 8, 9); 0.9, 0.1, 0.1⟩	6.75
8	⟨(7, 8, 9, 9); 0.85, 0.1, 0.15⟩	7.15
9	⟨(9, 9, 9, 9); 1, 0, 0⟩	9

Step 5: Opinions of DMs are aggregated in matrices created with SVTNNs. To aggregate the views of more than one DM, the TNWAA operator is used, as shown in Eq. (9).

Step 6: Neutrosophic synthetic values are calculated. This step is calculated according to the following equation.

$$S_i = \sum_{j=1}^{n} n_{ij} \times \left[\sum_{i=1}^{n}\sum_{j=1}^{n} n_{ij}\right]^{-1}, i = 1, \ldots, n, \tag{13}$$

where n is the number of elements and η_{ij} is the *(i, j)th* element of the clustered pairwise comparison matrix.

Step 7: In the final stage, the final weights of importance are determined. The weights are calculated based on eq. (14) below, and the equation in Definition (7) is used to compare the weights.

$$W_i = \frac{S_i}{\sum_{i=1}^{n} S_i}, i = 1, \ldots, n. \tag{14}$$

3.4. Reclassification of Parameters and Flood Susceptibility Mapping

Each of the eleven thematic layers prepared is divided into various classes. Subunits of the parameters were rated as having importance in influencing flood formation. In the rating process, the threshold values in the common literature and the general geographical characteristics of the research area were considered. The thematic layers are divided into five categories (excluding lithology and NDVI) (1 = very low impact, and 5 = very high impact).

The ArcGIS program converted Each parametric layer to 30 × 30 m raster format. The ratings given to each parameter class were used by the "Reclass" module to generate the layers. Drawing the final flood risk susceptibility map of the Melet Basin was made possible by combining the various layers using the "Map Calculator" module. The following formula generated the iterative flood risk index (FHI) computation:

$$FHI = \sum_{i=1}^{n} W_i F_i \tag{15}$$

where W_i corresponds to the weight of each factor, F_i is the rating factor, and n is the number of parameters.

Finally, the resulting flood risk map was reclassified into five groups; very high, high, medium, low and very low using Natural Break Jenks (Arabameri et al., 2019; Mudashiru et al., 2022b). Natural Breaks (Jenks) method is a data classification technique used in GIS and spatial statistics. It is used to group similar values in a data set into a set of classes or clusters based on their statistical properties (Lu et al., 2021).

4. Results and Discussion

In the study, thematic maps of 11 parameters were first produced and reclassified. The class range values of the thematic maps produced and the tables and texts showing the share of the said value range in the basin's total area are given below. The elevation of the research area is divided into five categories according to its impact on flood hazards: Very high (2250 m and above), high (1500–2250 m), medium (750–1500 m), low (250–750 m) and very low (250 m and below). Each class covers approximately 3.14%, 41.46%, 38.57%, 13.38% and 3.45% of the total catchment area, respectively (Table 4; Figure 3). Cultivated lands constitute 32.18% of the basin's land use, while structuring is 0.46%, and wetland, bare and forest areas are 0.51%, 32.54%, and 34.31%, respectively (Table 4; Figure 7). Denser vegetation can reduce an area's vulnerability to flooding. The NDVI layer is divided into low (-1) and high (1). While 17.33% of the basin is low-class land, 82.67% is high-class land (Table 4; Figure 7). It is divided into five classes according to the effect on soil type risk: very high (sandy clay loam), high (clay), medium (sandy loam), low (clay loam) and very low (loam). Each class covers approximately 0.20%, 3.29%, 0.05%, 38.22% and 58.24% of the total catchment area, respectively (Table 4; Figure 8). Detailed findings for other parameters are included in Table 4.

Table 4: Selected parameters of flood susceptibility of Melet Basin

Criteria	Classes	Reclas sclass	Area (km^2)	Rate (%)	Criteria	Classes	Reclas sclass	Area (km^2)	Rate (%)
Elevation	< 250	5	68	3,45	Topographic wetness index (TWI)	2.48–5.91	1	1123	56,92
	250-750	4	264	13,38		5.91–8.09	2	336	17,03
	750-1500	3	761	38,57		8.09–10.18	3	116	5,88
	1500-2250	2	818	41,46		10.18–12.63	4	77	3,90
	> 2250	1	62	3,14		12.63–22.77	5	321	16,27
Slope	< 6	5	205	10,39	Distance to stream	> 5	5	10	0,51
	6–12	4	385	19,51		5.10	4	10	0,51
	12-18	3	430	21,79		10.25	3	29	1,47
	18-36	2	866	43,89		25-50	2	48	2,43
	> 36	1	87	4,41		< 50	1	1876	95,08
Lithology	Sediment	4	16	0,81	Land use/landcover	Water body	5	10	0,51
	Volcanic	3	1338	67,82		Urban area	4	9	0,46
	Metamorphic	2	619	31,37		Bareland	3	642	32,54
Drainage density	> 6	5	158	8,01		Cultivated area	2	635	32,18
	4.5 – 6	4	470	23,82		Forest area	1	677	34,31
	3 – 4.5	3	698	35,38	NDVI	− 1	2	342	17,33
	1.5 – 3	2	434	22,00		1	4	1631	82,67
	< 1.5	1	213	10,80	Soil	Sandy clayloam	5	4	0,20
Average annual rainfall	<750	1	303	15,36		Clay	4	65	3,29
	750-1050	2	483	24,48		Sandy Loam	3	1	0,05
	1050-1350	3	876	44,40		Clay Loam	2	754	38,22
	1350-1650	4	293	14,85		Loam	1	1149	58,24
	1650 +	5	18	0,91					
Stream power index (SPI)	− 10 to − 8	1	1	0,05					
	− 7 to − 3	2	87	4,41					
	− 2 to − 0.9	3	261	13,23					
	− 0.8 to – 2	4	1584	80,28					
	3–8	5	40	2,03					

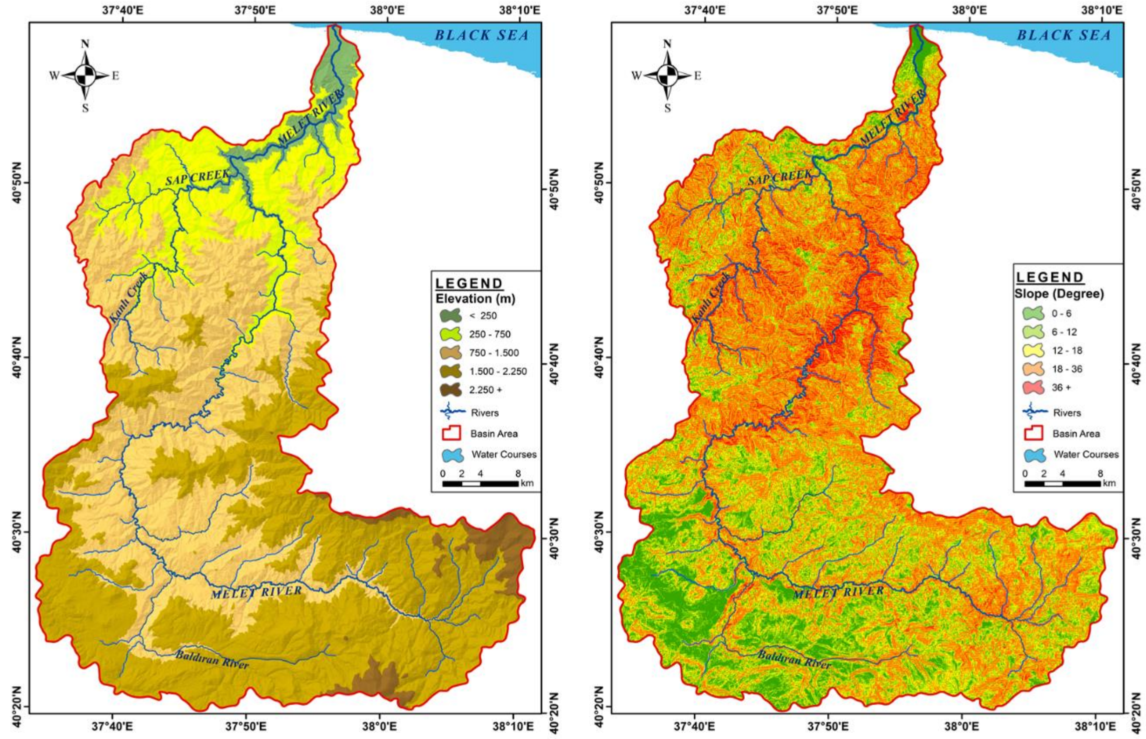

Figure 3: Tematic layers: elevation and slope

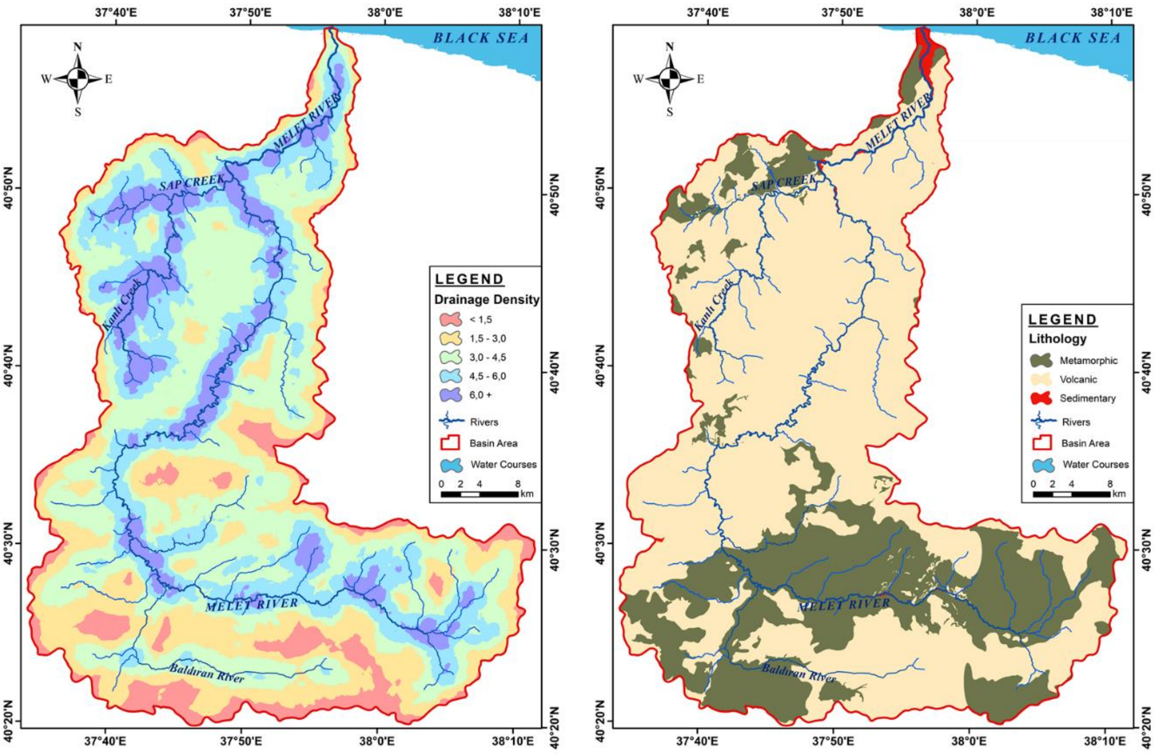

Figure 4: Tematic layers: lithology and drainage density

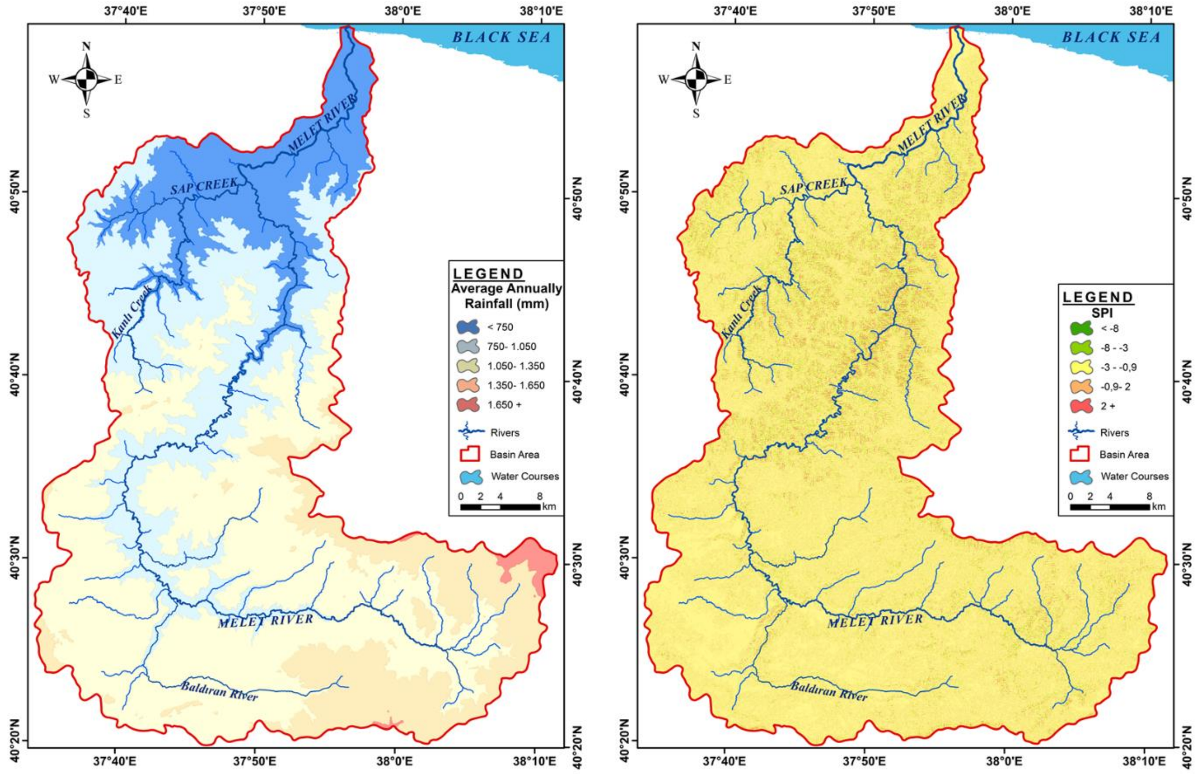

Figure 5: Tematic layers rainfall and SPI

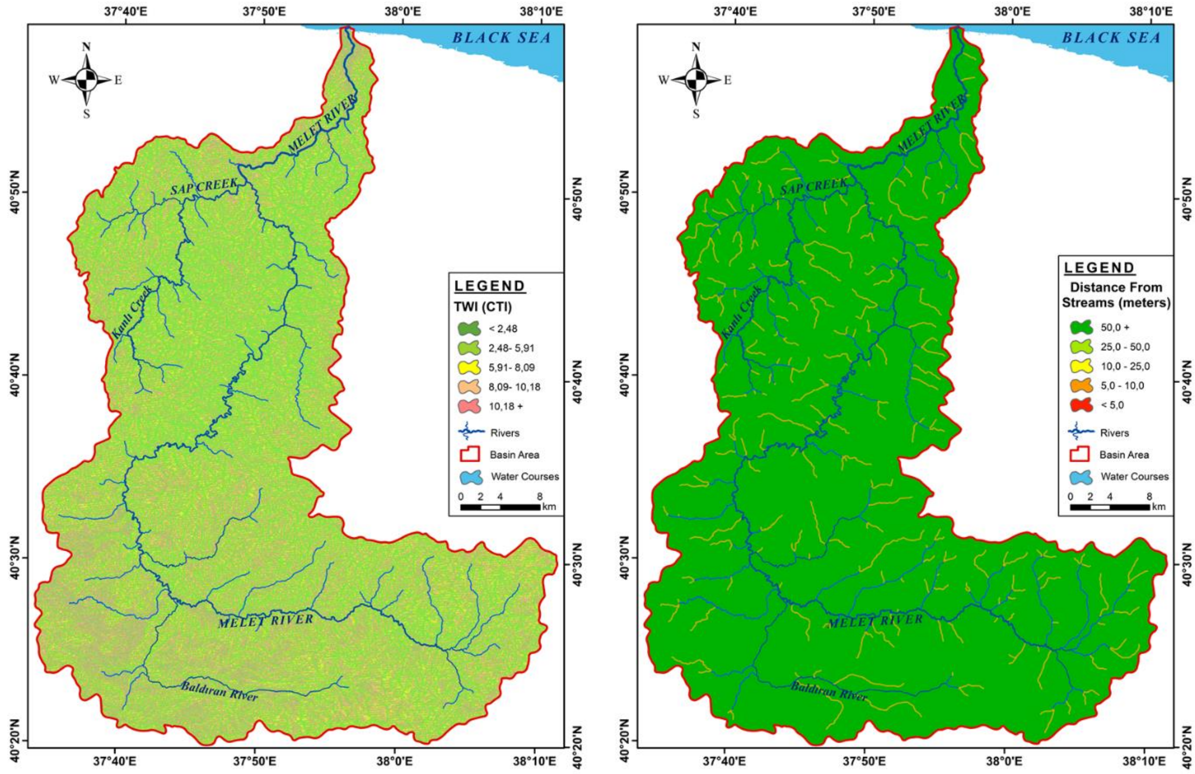

Figure 6. Tematic layers: TWI and distance from streams

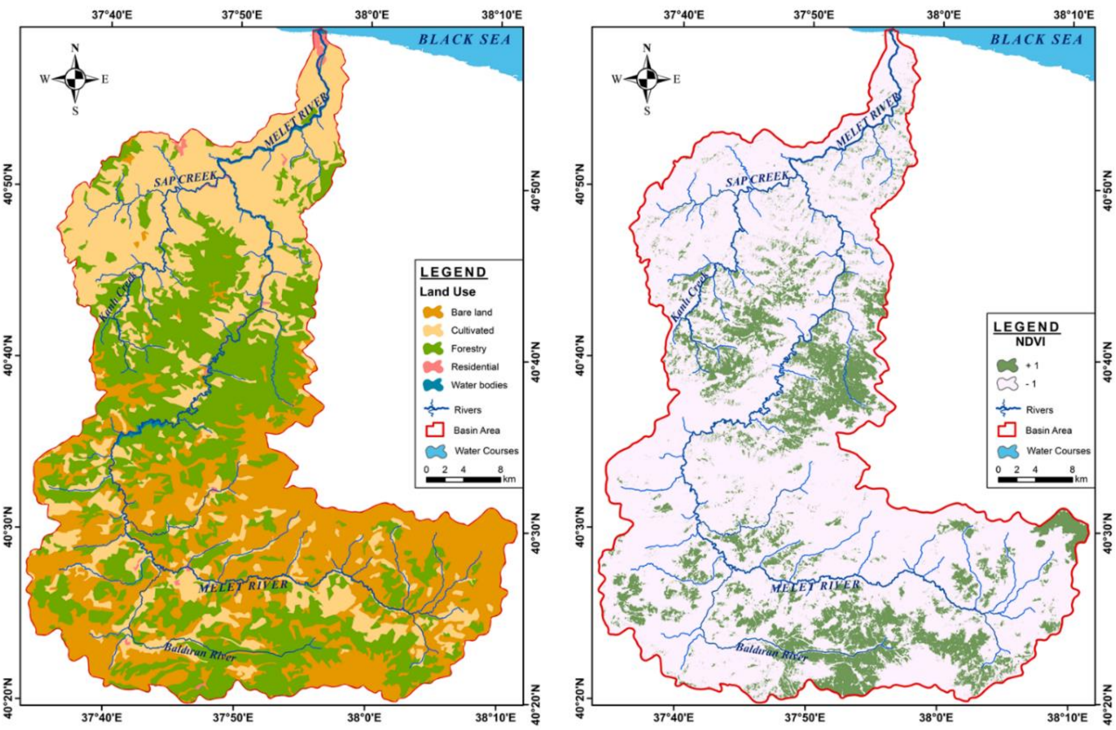

Figure 7: Tematic layers: Land use and NDVI

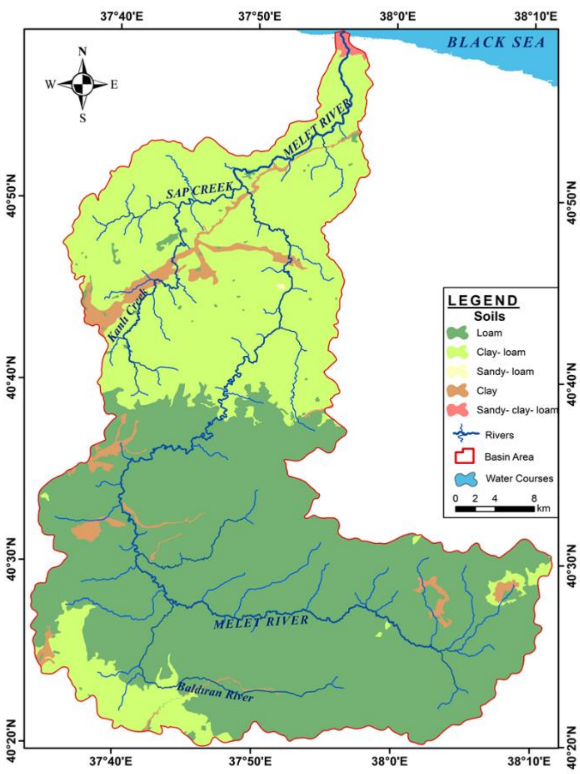

Figure 8: Tematic layers: soil

4.1. N-AHP- GIS Approach

Eleven factors were employed in this work to map flood hazards. The reclassification method splits each parameter into relevant subclasses. Then, the application steps of the neutrosophic fuzzy AHP were followed, and the weight values of the parameters were calculated. The normalized weight values were analyzed in the GIS tool to estimate the Flood Hazard Index using Equation (14). The main stages of the application are presented in detail below.

First, the NF-AHP technique was applied to obtain the weights of the parameters effective in floods. In the study, a DM group of four was determined to evaluate 11 parameters by pairwise comparisons. The DMs selection process was based on the participant's knowledge and expertise. DMs' short profiles are presented in Table 5. Each DM was assigned a weight of importance $\rho = (0.25, 0.35, 0.30, 0.10)^T$ according to their knowledge and experience. These weight values were then used in the aggregation calculations of the responses with the TNWAA operator.

Table 5: Weights of the DMs

DMs	**Expertise**	**Weights**
DM_1	Physical Geography, Geomorphology	0.25
DM_2	Natural disasters	0.35
DM_3	Natural Disasters, Risk Analysis	0.30
DM4	Geomorphology	0.10

Four DMs rated factors using the rating scale (1-9) given in Table 2. First, pairwise comparison matrices were created based on the data obtained as a result of the evaluations (Table 6).

Table 6: Initial decision matrix

DM_1	C_1	C_2	C_3	C_4	C_5	C_6	C_7	C_8	C_9	C_{10}	C_{11}
C_1-Elevation	1	1/5	1/3	1	1/7	4	1/5	1/6	1/4	1	1/5
C_2- *Slope*		1	1/3	4	5	1	1/4	1/3	1/2	3	1/4
C_3- Lithology			1	1	1/3	1	1/5	1/5	1	1	1/4
C_4- Drainage density				1	1/3	1/4	1/2	1/6	1/4	3	1/5
C_5- Average annual rainfall					1	1	1	1/4	2	3	1/3
C_6- *SPI*						1	1	1	3	5	1
C_7- *TWI*							1	1	5	6	4
C_8- Distance to stream								1	4	6	1/2
C_9- *LULC*									1	6	1/4
C_{10}- *NDVI*										1	1/5
C_{11}- *Soil*											1
DM_2	C_1	C_2	C_3	C_4	C_5	C_6	C_7	C_8	C_9	C_{10}	C_{11}
C_1-Elevation	1	1/7	1/2	0	1/2	1/5	1/5	1/7	1/5	1/5	5
C_2- *Slope*		1	1/3	4	5	1	1/4	1/3	1/2	3	1/4
C_3- Lithology			1	1	1/3	1	1/5	1/5	1	1	1/4
C_4- Drainage density				1	1/3	1/4	1/2	1/6	1/4	3	1/5
C_5- Average annual rainfall					1	1	1	1/4	2	3	1/3
C_6- *SPI*						1	1	1	3	5	1
C_7- *TWI*							1	1	5	6	4
C_8- Distance to stream								1	4	6	1/2
C_9- *LULC*									1	6	1/4
C_{10}- *NDVI*										1	1/5
C_{11}- *Soil*											1
DM_3	C_1	C_2	C_3	C_4	C_5	C_6	C_7	C_8	C_9	C_{10}	C_{11}
C_1-Elevation	1	1/7	1/2	0	1/2	1/5	1/5	1/7	1/5	1/5	5
C_2- *Slope*		1	1/3	4	5	1	1/4	1/3	1/2	3	1/4
C_3- Lithology			1	1	1/3	1	1/5	1/5	1	1	1/4
C_4- Drainage density				1	1/3	1/4	1/2	1/6	1/4	3	1/5
C_5- Average annual rainfall					1	1	1	1/4	2	3	1/3
C_6- *SPI*						1	1	1	3	5	1
C_7- *TWI*							1	1	5	6	4
C_8- Distance to stream								1	4	6	1/2
C_9- *LULC*									1	6	1/4
C_{10}- *NDVI*										1	1/5
C_{11}- *Soil*											1
DM_4	C_1	C_2	C_3	C_4	C_5	C_6	C_7	C_8	C_9	C_{10}	C_{11}
C_1-Elevation	1	1/7	1/2	0	1/2	1/5	1/5	1/7	1/5	1/5	5
C_2- *Slope*		1	1/3	4	5	1	1/4	1/3	1/2	3	1/4
C_3- Lithology			1	1	1/3	1	1/5	1/5	1	1	1/4
C_4- Drainage density				1	1/3	1/4	1/2	1/6	1/4	3	1/5
C_5- Average annual rainfall					1	1	1	1/4	2	3	1/3
C_6- *SPI*						1	1	1	3	5	1
C_7- *TWI*							1	1	5	6	4
C_8- Distance to stream								1	4	6	1/2
C_9- *LULC*									1	6	1/4
C_{10}- *NDVI*										1	1/5
C_{11}- *Soil*											1

The CR values of the first pairwise comparison matrices were calculated using equation (11), and the CR values for all matrices were below 10%.

Then, the values in the first pairwise comparison matrices obtained on a scale of 1-9 were converted to SVTNNs in Table 3. In the next step, the TNWAA operator is used, as shown in equation (8), to aggregate the views of more than one DM in the matrices created with SVTNN. In Table 7, the combined decision matrix of all factors is given.

Table 7: Aggregated decision matrix

	C_1	C_2	C_3
C_1	⟨(1.00, 1.00, 1.00, 1.00); 0.50, 0.50, 0.50⟩	⟨(1.17, 1.59, 2.20, 2.62); 1.00, 0.00, 0.00⟩	⟨(0.63, 0.91, 1.82, 2.35); 1.00, 0.00, 0.00⟩
C_2	⟨(3.17, 3.78, 4.41, 3.65); 1.00, 0.00, 0.00⟩	⟨(1.00, 1.00, 1.00, 1.00); 0.50, 0.50, 0.50⟩	⟨(3.96, 4.22, 4.98, 5.25); 1.00, 0.00, 0.00⟩
C_3	⟨(1.09, 1.84, 3.68, 5.88); 1.00, 0.00, 0.00⟩	⟨(0.57, 0.68, 1.02, 1.16); 1.00, 0.00, 0.00⟩	⟨(1.00, 1.00, 1.00, 1.00); 0.50, 0.50, 0.50⟩
C_4	⟨(3.55, 4.25, 4.95, 5.65); 0.75, 0.23, 0.25⟩	⟨(2.09, 2.50, 2.90, 3.31); 1.00, 0.00, 0.00⟩	⟨(1.95, 2.21, 2.47, 2.74); 1.00, 0.00, 0.00⟩
C_5	⟨(3.15, 4.15, 5.50, 6.50); 0.73, 0.24, 0.34⟩	⟨(2.00, 2.75, 3.85, 4.60); 0.53, 0.46, 0.47⟩	⟨(4.60, 5.60, 6.60, 7.60); 0.82, 0.16, 0.18⟩
C_6	⟨(1.97, 2.58, 3.70, 4.32); 1.00, 0.00, 0.00⟩	⟨(0.51, 0.63, 0.93, 1.21); 1.00, 0.00, 0.00⟩	⟨(0.91, 1.52, 2.99, 3.62); 1.00, 0.00, 0.00⟩
C_7	⟨(2.35, 3.00, 4.25, 4.90); 0.60, 0.37, 0.00⟩	⟨(1.51, 1.93, 2.66, 3.28); 1.00, 0.00, 0.00⟩	⟨(2.35, 3.25, 4.50, 5.40); 0.60, 0.36, 0.40⟩
C_8	⟨(4.35, 5.35, 6.60, 7.60); 0.76, 0.23, 0.22⟩	⟨(2.74, 3.40, 4.55, 5.21); 1.00, 0.00, 0.00⟩	⟨(2.45, 3.20, 4.75, 5.50); 0.58, 0.39, 0.42⟩
C_9	⟨(3.05, 3.80, 4.75, 5.50); 0.71, 0.24, 0.29⟩	⟨(1.69, 2.10, 2.70, 3.11); 1.00, 0.00, 0.00⟩	⟨(1.50, 2.20, 3.35, 4.05); 0.49, 0.51, 0.51⟩
C_{10}	⟨(0.61, 0.88, 1.66, 1.96); 1.00, 0.00, 0.00⟩	⟨(0.94, 1.19, 1.94, 2.19); 1.00, 0.00, 0.00⟩	⟨(0.87, 1.14, 1.49, 1.87); 1.00, 0.00, 0.00⟩
C_{11}	⟨(1.60, 2.26, 3.22, 3.93); 1.00, 0.00, 0.00⟩	⟨(0.78, 1.10, 2.01, 2.34); 1.00, 0.00, 0.00⟩	⟨(0.61, 0.74, 1.14, 1.43); 1.00, 0.00, 0.00⟩
	C_4	C_5	C_6
C_1	⟨(0.39, 0.41, 0.42, 0.45); 1.00, 0.00, 0.00⟩	⟨(0.16, 0.19, 0.30, 0.50); 1.00, 0.00, 0.00⟩	⟨(1.38, 1.80, 2.25, 2.71); 1.00, 0.00, 0.00⟩
C_2	⟨(2.41, 2.76, 3.13, 3.49); 1.00, 0.00, 0.00⟩	⟨(0.38, 0.41, 0.52, 0.72); 1.00, 0.00, 0.00⟩	⟨(1.67, 2.28, 3.25, 3.90); 1.00, 0.00, 0.00⟩
C_3	⟨(1.83, 2.18, 2.54, 2.89); 1.00, 0.00, 0.00⟩	⟨(0.14, 0.16, 0.19, 0.24); 1.00, 0.00, 0.00⟩	⟨(1.51, 1.93, 2.46, 3.08); 1.00, 0.00, 0.00⟩
C_4	⟨(1.00, 1.00, 1.00, 1.00); 0.50, 0.50, 0.50⟩	⟨(0.79, 1.54, 3.08, 3.88); 1.00, 0.00, 0.00⟩	⟨(3.80, 4.80, 6.30, 7.30); 0.72, 0.27, 0.28⟩
C_5	⟨(0.65, 0.94, 1.88, 2.50); 1.00, 0.00, 0.00⟩	⟨(1.00, 1.00, 1.00, 1.00); 0.50, 0.50, 0.50⟩	⟨(4.40, 5.40, 6.40, 7.40); 0.76, 0.18, 0.24⟩
C_6	⟨(0.14, 0.17, 0.23, 0.32); 1.00, 0.00, 0.00⟩	⟨(0.14, 0.16, 0.19, 0.23); 1.00, 0.00, 0.00⟩	⟨(1.00, 1.00, 1.00, 1.00); 0.50, 0.50, 0.50⟩
C_7	⟨(0.39, 0.41, 0.42, 0.45); 1.00, 0.00, 0.00⟩	⟨(0.15, 0.18, 0.24, 0.33); 1.00, 0.00, 0.00⟩	⟨(1.35, 2.01, 3.97, 4.64); 1.00, 0.00, 0.00⟩
C_8	⟨(0.48, 0.50, 0.52, 0.55); 1.00, 0.00, 0.00⟩	⟨(0.19, 0.23, 0.43, 0.81); 1.00, 0.00, 0.00⟩	⟨(2.80, 3.80, 6.00, 7.00); 0.58, 0.39, 0.42⟩
C_9	⟨(1.55, 2.45, 4.80, 5.70); 0.36, 0.69, 0.64⟩	⟨(0.53, 0.90, 1.66, 2.08); 1.00, 0.00, 0.00⟩	⟨(2.76, 3.42, 4.09, 4.77); 1.00, 0.00, 0.00⟩
C_{10}	⟨(0.18, 0.22, 0.34, 0.56); 1.00, 0.00, 0.00⟩	⟨(0.16, 0.19, 0.23, 0.30); 1.00, 0.00, 0.00⟩	⟨(0.60, 0.72, 1.05, 1.20); 1.00, 0.00, 0.00⟩
C_{11}	⟨(0.40, 0.43, 0.50, 0.61); 1.00, 0.00, 0.00⟩	⟨(0.14, 0.17, 0.25, 0.34); 1.00, 0.00, 0.00⟩	⟨(1.19, 1.60, 2.60, 3.01); 1.00, 0.00, 0.00⟩
	C_7	C_8	C_9
C_1	⟨(0.44, 0.46, 0.52, 0.59); 1.00, 0.00, 0.00⟩	⟨(0.14, 0.16, 0.24, 0.39); 1.00, 0.00, 0.00⟩	⟨(0.36, 0.38, 0.41, 0.46); 1.00, 0.00, 0.00⟩
C_2	⟨(0.91, 1.52, 2.99, 3.63); 1.00, 0.00, 0.00⟩	⟨(2.18, 2.55, 2.94, 3.35); 1.00, 0.00, 0.00⟩	⟨(2.41, 2.77, 3.14, 3.53); 1.00, 0.00, 0.00⟩
C_3	⟨(0.26, 0.29, 0.40, 0.61); 1.00, 0.00, 0.00⟩	⟨(0.36, 0.63, 1.20, 0.79); 1.00, 0.00, 0.00⟩	⟨(0.43, 0.46, 0.59, 0.83); 1.00, 0.00, 0.00⟩
C_4	⟨(3.80, 4.50, 5.20, 5.90); 0.79, 0.19, 0.21⟩	⟨(2.80, 3.40, 4.00, 4.60); 0.71, 0.24, 0.29⟩	⟨(0.25, 0.28, 0.46, 0.73); 1.00, 0.00, 0.00⟩
C_5	⟨(3.30, 4.30, 5.80, 6.80); 0.65, 0.30, 0.35⟩	⟨(1.75, 2.75, 4.50, 5.50); 0.54, 0.45, 0.46⟩	⟨(1.52, 2.09, 3.33, 4.05); 1.00, 0.00, 0.00⟩
C_6	⟨(1.49, 1.86, 2.31, 2.78); 1.00, 0.00, 0.00⟩	⟨(0.14, 0.17, 0.28, 0.40); 1.00, 0.00, 0.00⟩	⟨(1.14, 1.51, 1.88, 2.26); 1.00, 0.00, 0.00⟩
C_7	⟨(1.00, 1.00, 1.00, 1.00); 0.50, 0.50, 0.50⟩	⟨(0.44, 0.81, 1.60, 2.05); 1.00, 0.00, 0.00⟩	⟨(0.79, 1.16, 2.26, 2.68); 1.00, 0.00, 0.00⟩
C_8	⟨(1.57, 2.24, 4.08, 4.90); 1.00, 0.00, 0.00⟩	⟨(1.00, 1.00, 1.00, 1.00); 0.50, 0.50, 0.50⟩	⟨(1.25, 1.85, 3.30, 3.90); 0.42, 0.61, 0.58⟩
C_9	⟨(2.15, 2.81, 4.02, 4.73); 1.00, 0.00, 0.00⟩	⟨(0.51, 0.53, 0.66, 0.88); 1.00, 0.00, 0.00⟩	⟨(1.00, 1.00, 1.00, 1.00); 0.50, 0.50, 0.50⟩
C_{10}	⟨(0.22, 0.25, 0.36, 0.48); 1.00, 0.00, 0.00⟩	⟨(0.17, 0.21, 0.36, 0.62); 1.00, 0.00, 0.00⟩	⟨(0.17, 0.20, 0.31, 0.52); 1.00, 0.00, 0.00⟩
C_{11}	⟨(0.49, 0.51, 0.58, 0.66); 1.00, 0.00, 0.00⟩	⟨(0.14, 0.17, 0.19, 0.25); 1.00, 0.00, 0.00⟩	⟨(0.17, 0.21, 0.32, 0.54); 1.00, 0.00, 0.00⟩
	C_{10}	C_{11}	
C_1	⟨(2.84, 3.59, 4.38, 5.18); 1.00, 0.00, 0.00⟩	⟨(0.82, 1.19, 2.32, 2.82); 1.00, 0.00, 0.00⟩	
C_2	⟨(3.59, 3.59, 3.63, 3.68); 1.00, 0.00, 0.00⟩	⟨(3.24, 3.85, 4.50, 5.15); 1.00, 0.00, 0.00⟩	
C_3	⟨(1.74, 2.50, 4.06, 4.83); 1.00, 0.00, 0.00⟩	⟨(1.41, 2.02, 2.98, 3.60); 1.00, 0.00, 0.00⟩	
C_4	⟨(2.30, 3.30, 4.65, 5.65); 0.54, 0.43, 0.46⟩	⟨(2.30, 3.00, 4.30, 5.00); 0.60, 0.37, 0.40⟩	
C_5	⟨(3.35, 4.35, 5.35, 6.35); 0.69, 0.26, 0.31⟩	⟨(3.30, 4.30, 6.00, 7.00); 0.69, 0.26, 0.31⟩	
C_6	⟨(2.11, 2.72, 3.33, 3.95); 1.00, 0.00, 0.00⟩	⟨(2.41, 2.77, 3.17, 3.58); 1.00, 0.00, 0.00⟩	
C_7	⟨(2.65, 3.55, 5.75, 6.65); 0.45, 0.55, 0.55⟩	⟨(1.85, 2.45, 3.75, 4.35); 0.47, 0.53, 0.53⟩	
C_8	⟨(2.35, 3.35, 5.65, 6.65); 0.42, 0.57, 0.58⟩	⟨(4.40, 5.40, 6.40, 7.40); 0.81, 0.17, 0.19⟩	
C_9	⟨(2.90, 3.90, 5.25, 6.25); 0.67, 0.30, 0.33⟩	⟨(2.65, 3.65, 5.00, 6.00); 0.64, 0.32, 0.36⟩	
C_{10}	⟨(1.00, 1.00, 1.00, 1.00); 0.50, 0.50, 0.50⟩	⟨(0.45, 0.83, 1.61, 2.08); 1.00, 0.00, 0.00⟩	
C_{11}	⟨(1.52, 2.19, 3.63, 4.45); 1.00, 0.00, 0.00⟩	⟨(1.00, 1.00, 1.00, 1.00); 0.50, 0.50, 0.50⟩	

Then, the neutrosophic synthetic values were calculated by applying Equation (12) to the combined matrix obtained. In the final stage, the factors' final weights were estimated using Equation (13) (Table 8).

Table 8: The weights of the criteria

No	Criteria	SVTNN weights	Crisp	Normalised	%
C1	Elevation	⟨(0.013, 0.027, 0.094, 0.212); 1, 0, 0⟩	0,086	0,051	5,1
C2	Slope	⟨(0.033, 0.066, 0.204, 0.414); 1, 0, 0⟩	0,179	0,106	10,6
C3	Lithology	⟨(0.014, 0.032, 0.119, 0.276); 1, 0, 0⟩	0,110	0,065	6,5
C4	Drainage density	⟨(0.033, 0.071, 0.232, 0.508); 1, 0, 0⟩	0,211	0,125	12,5
C5	Average annual rainfall	⟨(0.039, 0.087, 0.296, 0.625); 1, 0, 0⟩	0,262	0,155	15,5
C6	Stream power index (SPI)	⟨(0.016, 0.035, 0.118, 0.263); 1, 0, 0⟩	0,108	0,064	6,4
C7	Topographic wetness index (TWI)	⟨(0.020, 0.046, 0.179, 0.396); 1, 0, 0⟩	0,160	0,095	9,5
C8	Distance to stream	⟨(0.032, 0.070, 0.255, 0.560); 1, 0, 0⟩	0,229	0,136	13,6
C9	Landuse/landcover	⟨(0.027, 0.062, 0.220, 0.489); 1, 0, 0⟩	0,199	0,118	11,8
C10	NDVI	⟨(0.007, 0.016, 0.061, 0.142); 1, 0, 0⟩	0,056	0,034	3,4
C11	Soil	⟨(0.011, 0.024, 0.091, 0.206); 1, 0, 0⟩	0,083	0,049	4,9

Ultimately, all parameters were transformed into a raster format by utilising a raster calculator in ArcGIS to superimpose each raster layer depending on the weights acquired using the NF-AHP technique and setting the spatial resolution of each raster layer to a cell size of 30 m × 30 m. This technique produced an integrated database with five flood susceptibility classes. These:

– Very low flood risk class representing 4.2% (83 km^2) of the watershed;
– Low flood class covering 43.34% (855 km^2) of the basin and covering a large area throughout the basin;
– Middle flood class covering 41.87% (826 km^2) of the basin;
– High flood class covering 9.88% (195 km^2) of the basin;
– It is a very high flood class, corresponding to 0.71% of the basin.

Table 9: Flood susceptibility, area coverage and percentage

Risk Status	Class	Area (km^2)	Ratio (%)
Very Low	1	83	4,21
Low	2	855	43,34
Medium	3	826	41,87
High	4	195	9,88
Very High	5	14	0,71
Sum		**1973**	**100**

According to the spatial findings of the study, the very low flood class is mainly distributed in areas far from the main drainage networks. Along with the low, the medium flood class corresponds to 85% of the basin. The regions corresponding to the high to very high flood class tend to be concentrated primarily in the city centre of Ordu, which is located at the sea level of the basin, and in the upper reaches of the basin, where both the elevation is high, and the leading drainage network is dense. The findings showed that 10% of the basin has a high flood potential. In Hatipoğlu (2017)'s study, which deals with the lower and middle course of the basin, they determined a high flood class of 1%. The first reason for this proportional difference in both studies is the inclusion of the basin in the upper course of the current research; secondly, in Hatipoğlu (2017)'s analysis, the parameters were individually weighted to be completed on the face. In the present study, it can be explained that weighting the parameters with NF-AHP provides more objective results.

Through factor grading, precipitation, distance from the river, drainage density, LULC and slope were found to be the most important factors affecting flooding, contributing approximately 74%. In comparison, combining the other five layers contributed 26% to flood risk. These findings are partially consistent with those obtained by similar studies (Morea & Samanta, 2020; Tella & Balogun, 2020; Hagos et al., 2022; Penki et al., 2022) in the literature. For example, Hagos et al. (2022) found that slope, drainage density, distance from the river and precipitation are the most important parameters in flood formation in their Ethiopian Awash River basin study. Apart from these, the LULC factor has been an important flood parameter of the basin in the current study. This finding is consistent with the results of Nsangou et al. (2022), Vaddiraju and Talari (2022), and Ghosh and Kar (2018) about LULC forming an important flood parameter. Among these five factors that most affect flood events in the region, LULC has undergone a significant change in recent years. In particular, the flat areas in the lower part of the basin have been a rapid urban expansion area. According to Şenol (2019a), the settlement areas, which covered an area of 2.3 km^2 in 1990, increased to 38 km^2 2018 throughout the basin. This change caused a high level of soil impermeability (Das, 2019) and increased the flood risk in residential areas.

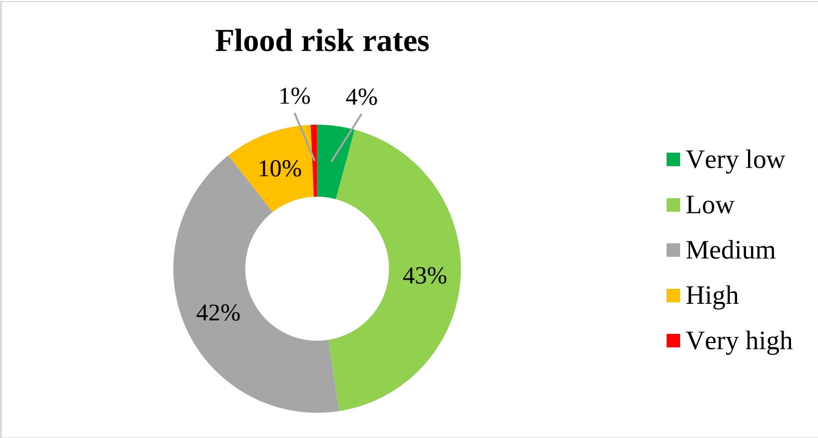

Figure 9: Flood risk rates chart

4.2. Validation

The final stage of flood susceptibility studies is the making of verification maps. In the current study, a verification map was produced by combining the last flood risk sensitivity map with the locations of the floods that occurred in the past. When the map is examined, it is seen that the floods experienced in the past periods correspond to the high-risk and risky regions in the current research. It is seen that it is concentrated in the centre of Ordu province, which is located at the point where the basin spills into the sea. These results prove the validity of the NF-AHP approach proposed in the study of flood risk mapping.

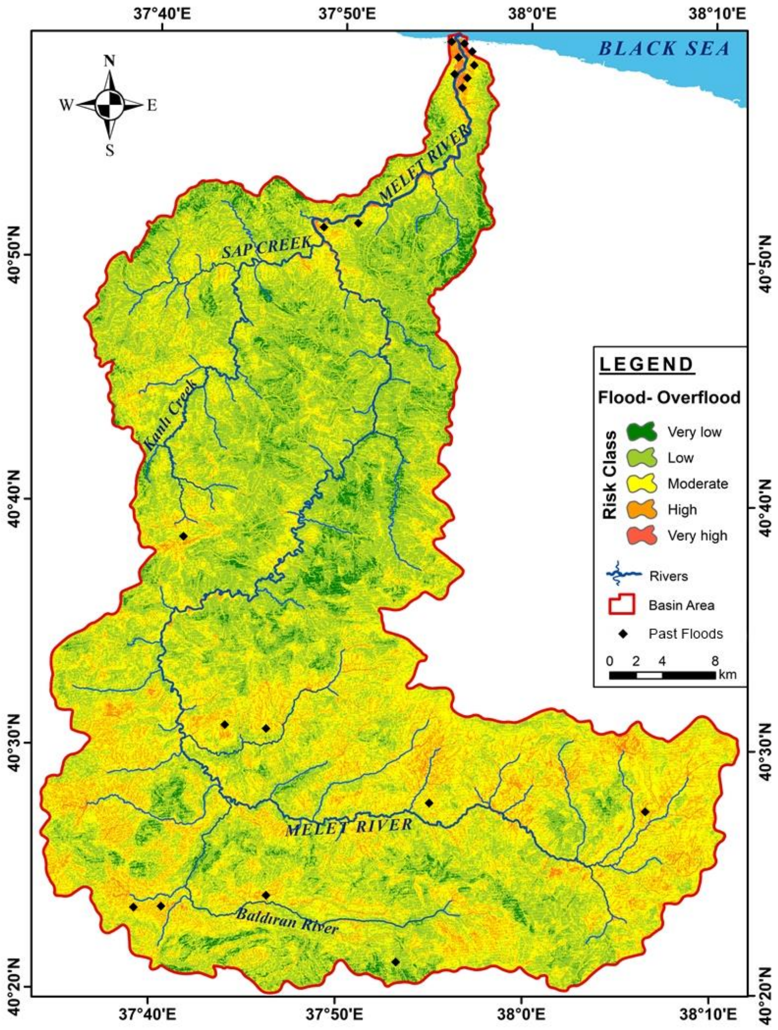

Figure 10: Flood inventory and flood susceptibility map of Melet Basin

5. Conclusion

As in the world, floods cause significant loss of life and property every year in Turkey. For this reason, developed flood simulations and risk assessment models can be used as a strategic planning tool to identify possible flood areas and reduce losses. In this context, the current study aimed to evaluate the flood sensitivity of the Melet River Basin with GIS-based MCDM. In weighting flood parameters, the N-AHP technique was used as an alternative to traditional AHP. It is stated that this technique can be a useful tool in minimizing the uncertainty and ambiguity encountered in the expert evaluation and in obtaining more objective results.

The elevation, precipitation, slope, aspect, TWI, SPI, drainage density, lithology, soil, precipitation, and distance from streams were among the inputs used by the N-AHP model to map flood vulnerability. The analysis revealed that the main variables influencing flooding in the basin were slope, LULC, drainage density, distance from the river, and precipitation. In addition, risky flood areas of the basin were verified against data from previous floods. It has been observed that the suggested NF-AHP technique can be a valuable tool for determining flood risk regions and creating maps of flood susceptibility. The study's maps can be used as a reference by planners, developers, and local and federal governments to help them prepare for and prevent flooding. It is expected that the results may aid different stakeholders in precisely identifying regions that are vulnerable to flooding and putting in place suitable flood control measures in such locations. Finally, the current study's results can be used as a reference for managing flood vulnerability in the Melet Basin. National and local governments can learn about high-risk areas to contain floods and improve flood prevention systems.

References

Abdel-Basset, M., Mohamed, M., & Smarandache, F. (2018a). An extension of neutrosophic AHP–SWOT analysis for strategic planning and decision-making. *Symmetry, 10*, Article 116. https://doi.org/10.3390/sym10040116

Abdel-Basset, M., Manogaran, G., Gamal, A., & Smarandache, F. (2018b). A hybrid approach of neutrosophic sets and DEMATEL method for developing suppliers election criteria. *Design Automation for Embedded Systems*, *22*, 257–278. https://doi.org/10.1007/s10617-018-9203-6

Ahmad, S. S., & Simonovic, S. P. (2011). A three-dimensional fuzzy methodology for flood risk analysis. *Journal Flood Risk Management*, *4*, 53–74. https://doi.org/10.1111/j.1753-318X.2011.01090.x

Arabameri, A., Rezaei, K., Cerdà, A., Conoscenti, C., & Kalantari, Z. (2019). A comparison of statistical methods and multi-criteria decision making to map flood hazard susceptibility in Northern Iran. *Science of the Total Environment*, *660*, 443–458. https://doi.org/10.1016/j.scitotenv.2019.01.021

Arca, D., & Yalçın, F. (2023). Production of flood risk maps of İnebolu Basin using different fuzzy analytic hierarchy process methods. *Journal of Disaster and Risk*, *6*(1), 70-83. https://doi.org/10.35341/afet.1137083

Aydın, M. C., & Birincioğlu, E. S. (2022). Flood risk analysis using gis-based analytical hierarchy process: a case study of Bitlis Province. *Applied Water Science*, *12*, Article 122. https://doi.org/10.1007/s13201-022-01655-x

Cai, S., Fan, J., & Yang, W. (2021). Flooding risk assessment and analysis based on GIS and the TFN-AHP method: a case study of Chongqing, China. *Atmosphere*, *12*(5), Article 623. https://doi.org/10.3390/atmos12050623

Cai, T., Li, X., Ding, X., Wang, J., & Zhan, J. (2019). Flood risk assessment based on hydrodynamic model and fuzzy comprehensive evaluation with GIS technique. *International Journal of Disaster Risk Reduction*, *35*, Article 101077. https://doi.org/10.1016/j.ijdrr.2019.101077

Chen, Y., Zhou, H., Zhang, H., Du, G., & Zhou, J. (2015). Urban flood risk warning under rapid urbanization. *Environmental Research*, *139*, 3-10. https://doi.org/10.1016/j.envres.2015.02.028

Das, S. (2019). Geospatial mapping of flood susceptibility and hydro-geomorphic response to the floods in Ulhas basin, India. *Remote Sensing Applications: Society and Environment, 14*, 60–74. https://doi.org/10.1016/j.rsase.2019.02.006

Deli, I., & Subas, Y. (2014). Single valued neutrosophic numbers and their applications to multicriteria decision making problem. *Neutrosophic Sets and Systems*, *2*(1), 1–13.

Ekmekçioğlu, Ö., Koç, K., & Özger, M. (2021). District based flood risk assessment in Istanbul using fuzzy analytical hierarchy process. *Stochastic Environmental Research and Risk Assessment*, *35*, 617–637. https://doi.org/10.1007/s00477-020-01924-8

Foudi, S., Osés-Eraso, N., & Tamayo, I. (2015). Integrated spatial flood risk assessment: the case of Zaragoza. *Land Use Policy*, *42*, 278–292. https://doi.org/10.1016/j.landusepol.2014.080.002

Ghosh, A., & Kar, S.K. (2018). Application of analytical hierarchyprocess (AHP) for flood risk assessment: a case study in Malda district of West Bengal, India. *Natural Hazards*, *94*, 349–368. https://doi.org/10.1007/s11069-018-3392-y

Hagos, Y.G., Andualem, T.G., Yibeltal, M., & Mengie, M.A. (2022). Flood hazard assessment and mapping using GIS integrated with multi-criteria decision analysis in upper Awash River basin, Ethiopia. *Applied Water Science*, *12*(7), 1–18. https://doi.org/10.1007/s13201-022-01674-8

Hammami, S., Zouhri, L., Souissi, D., Souei, A., Zghibi, A., Marzougui, A., & Dlala, M. (2019). Application of the GIS based multi-criteria decision analysis and analytical hierarchy process (AHP) in the flood susceptibility mapping (Tunisia). *Arabian Journal of Geoscience, 12*, Article 653. https://doi.org/10.1007/s12517-019-4754-9

Hategekimana, Y., Yu, L., Nie, Y., Zhu, J., Liu, F., & Guo, F. (2018). Integration of multi-parametric fuzzy analytic hierarchy process and GIS along the UNESCO World Heritage: a flood hazard index, Mombasa County, Kenya. *Natural Hazards, 92*, 1137–1153. https://doi.org/10.1007/s11069-018-3244-9

Hatipoğlu, İ.K. (2017). *Applied geomorphology of the lower and middle Melet River Melet, Ordu* [Doktora Tezi, Ondokuz Mayıs University]. YÖK Ulusal Tez Merkezi. https://tez.yok.gov.tr/UlusalTezMerkezi

Jun, K-S., Chung, E-S., Kim, Y-G., & Kim, Y. (2013). A fuzzy multi-criteria approach toflood risk vulnerability in South Korea by considering climate change impacts. *Expert Systems with Applications*, *40*, 1003–1013. https://doi.org/10.1016/j.eswa.2012.08.013

Kanani-Sadat, Y., Arabsheibani, R., Karimipour, F., & Nasseri, M. (2019). A new approach to flood susceptibility assessment in data-scarce and ungauged regions based on GIS-based hybrid multi criteria decision-making method. *Journal of Hydrology, 572*, 17–31. https://doi.org/10.1016/j.jhydrol.2019.02.034

Kaur, G., & Garg, H. (2022). A new method for image processing using generalized linguistic neutrosophic cubic aggregation operator. *Complex and Intelligent Systems, 8*, 4911–4937. https://doi.org/10.1007/s40747-022-00718-5

Keskin, İ. (2011). *1/100.000 scale Türkiye geological maps Perşembe-F39 and Giresun-G39 sheets*. MTA Publication.

Lai, C., Chen, X., Chen, X., Wang, Z., Wu, X., & Zhao, S. (2015). A fuzzy comprehensive evaluation model for flood risk based on the combination weight of game theory. *Natural Hazards*, *77*, 1243–1259. https://doi.org/10.1007/s11069-015-1645-6

Lappas, I., & Kallioras, A. (2019). Flood susceptibility assessment through GIS-based multi-criteria approach and analytical hierarchy process (AHP) in a River Basin in Central Greece. *International Research Journal of Engineering and Technology*, *6*(3), 738–751.

Li, C., Chai, Y., Yang, L., & Li, H. (2016). Spatio-temporal distribution of flooddisastersandanalysis of influencingfactors in Africa. *Natural Hazards*, *82*, 721–31. https://doi.org/10.1007/s11069-016-2181-8

Liu, Z., Merwade, V., & Jafarzadegan, K. (2019). Investigating the role of model structure and surface roughness in generating food in undation extents using one- and two-dimensional hydraulic models. *Journal of Flood Risk Management*, *12*(1), Article 12347. https://doi.org/10.1111/jfr3.12347

Lu, Y., He, T., Xu, X., & Qiao, Z. (2021). Investigation the robustness of standard classification methods for defining urban heat islands. *IEEE Journal of Selected Topics in Applied Earth Observations and Remote Sensing*, *14*, 11386–11394. https://doi.org/10.1109/JSTARS.2021.3124558

Lyu, H. M., Zhou, W. H., Shen, S. L., & Zhou, A. N. (2020). Inundation risk assessment of metro system using AHP and TFN-AHP in Shenzhen. *Sustainable Cities and Society*, *56*, Article 102103. https://doi.org/10.1016/j.scs.2020.102103

Mishra, K., & Sinha, R. (2020). Flood risk assessment in the Kosimega fan using multi-criteria decision analysis: a hydro-geomorphic approach. *Geomorphology, 350*, Article 106861. https://doi.org/10.1016/j.geomorph.2019.106861

Morea, H., & Samanta, S. (2020). Multi-criteria decision approach to identify flood vulnerability zones using geospatial technology in the kemp-welch catchment, Central Province. *Applied Geomatics*, *12*(4), 427–440. https://doi.org/10.1007/s12518-020-00315-6

Mudashiru, R. B., Sabtu, N., Abdullah, A., Saleh, A., & Abustan, I. (2022a). Optimality of flood influencing factors for flood hazard mapping: an evaluation of two multi-criteria decision-making methods. *Journal of Hydrology*, *612*, Article 128055. https://doi.org/10.1016/j.jhydrol.2022.128055

Mudashiru, R. B., Sabtu, N., Abdullah, R., Saleh, A., & Abustan, İ. (2022b). A comparison of three multi-criteria decision-making models in mapping flood hazard areas of Northeast Penang, Malaysia. *Natural Hazards*, *112*, 1903–1939. https://doi.org/10.1007/s11069-022-05250-w

Negese, A., Worku, D., Shitaye, A., & Getnet, H. (2022). Potential flood-prone area identification and mapping using GIS-based multi-criteria decision-making and analytical hierarchy process in Dega Damot district, Northwestern Ethiopia. *Applied Water Science*, *12*, 1–21, https://doi.org/10.1007/s13201-022-01772-7

Nsangou, D., Kpoumié, A., Mfonka, Z., Bateni, S. M., Ngouh, A. N., & NdamNgoupayou, J. R. (2022). The mfoundi watershed at yaoundé in the humid tropical zone of Cameroon: a case study of urban flood susceptibility mapping. *Earth System and Environment*, *6*, 99-120. https://doi.org/10.1007/s41748-021-00276-9

Özşahin, E. (2022). Havsa (Edirne) ilçesinde taşkın tehlike duyarlılığının değerlendirilmesi. In M. Tan, & T. Erdoğan (Eds). *Her Yönüyle Havsa*, (pp.711-732). Paradigma Akademi Yayınları.

Pappenberger, F., Matgen, P., Beven, K. J., Henry, J. B., & Pfister, L. (2006). Influence of uncertain boundary conditions and model structure on flood in undation predictions. *Advances in Water Resources*, *29*(10), 1430–1449. https://doi.org/10.1016/j.advwatres.2005.11.012

Penki, R., Basina, S. S., & Tanniru, S. R. (2022). Application of geographical information system-based analytical hierarchy process modeling for flood susceptibility mapping of Krishna District in Andhra Pradesh. *Environmental Science and Pollution Research*, *30*, 99062–99075. https://doi.org/10.1007/s11356-022-22924-x

Saaty, T.L. (1980). *The Analytic Hierarchy Process*. McGraw-Hill.

Saaty, T.L. (2005). *The oryand applications of the analytic network process: decision making with benefits, opportunities, costs, and risks.* RWS Publications.

Smarandache, F. (1999). *A unifying field in logic. Neutrosophy: neutrosophic probability, set, and logic*. American ResearchPress.

Souissi, D., Souie, A., Sebei, A., Mahfoudhi, R., Zghibi, A., Zouhri, L., Amiri, W., & Ghanmi, M. (2022). Flood hazard mapping and assessment using fuzzy analytic hierarchy process and GIS techniques in Takelsa, Northeast Tunisia. *Arabian Journal of Geoscience, 15*, Article 1405. https://doi.org/10.1007/s12517-022-10541-4

Stanujkić, D., Karabašević, D., Popović, G., Pamučar, D., Stević, Ž., Zavadskas, E. K., & Smarandache, F. (2021). A single-valued neutrosophic extension of the EDAS method. *Axioms, 1*0(4), Article 245. https://doi.org/10.3390/axioms10040245

Sümengen, M. (2013). *1/100.000 scale Türkiye geological maps Giresun-H40 sheet*. MTA Publication.

Şenol, C. (2019a). *Land use and spatial change in the Melet Stream Basin* [Doktora Tezi, Marmara Üniversitesi]. YÖK Ulusal Tez Merkezi. https://tez.yok.gov.tr/UlusalTezMerkezi

Şenol, C. (2019b). The situation of the spatial change in the lower part of the Melet River Basin is affected by potential flooding. *International Journal of Geography and Geography Education*, *40*, 439-453. https://doi.org/10.32003/iggei.571481

Taş, M.A., & Yanık, M.E. (2022). Flood risk analysis of behzat river (Tokat) basin with analytic hierarchy process (AHP) method. *Erzincan University Journal of Social Sciences Institute*, *15*(2), 185-199. https://doi.org/10.46790/erzisosbil.1221464

Tehrany, M. S., Lee, M. J., Pradhan, B., Jebur, M. N., & Lee, S. (2014). Flood susceptibility mapping using integrated bivariate and multivariate statistical models. *Environmental Earth Sciences*, *72*(10), 4001–4015. https://doi.org/10.1007/s12665-014-3289-3

Tella, A., & Balogun, A. L. (2020). Ensemble fuzzy MCDM for spatial assessment of flood susceptibility in Ibadan, Nigeria. *Natural Hazards, 104*, 2277–2306. https://doi.org/10.1007/s11069-020-04272-6

Toosi, A. S., Calbimonte, G. H., Nouri, H., & Alaghmand, S. (2019). River basin-scale flood hazard assessment using a modified multi-criteria decision analysis approach: a case study. *Jounal of Hydrology*, *574*, 660–671. https://doi.org/10.1016/j.jhydrol.2019.04.072

Tucker, C. (1979). Red and photographic infrared linear combination for monitoring vegetation of Environment. *Remote Sensing of Environment, 8,* 127-150. https://doi.org/10.1016/0034-4257(79)90013-0

Vaddiraju, S. C., & Talari, R. (2022). Urban flood susceptibility analysis of Saroor Nagar Watershed of Indiausing Geomatics-based multi-criteria analysis framework. *Environmental Science and Pollution Research*, *30*, 107021–107040. https://doi.org/10.1007/s11356-022-24672-4

Vafadarnikjoo, A. (2020). *Decision analysis in the UK energy supply chain risk management: Tools development and application* [Doctoral thesis, University of East Anglia]. https://ueaeprints.uea.ac.uk/id/eprint/77909

Vafadarnikjoo, A., BadriAhmadi, H., Liou, J. J. H., Botelho, T., & Chalvatzis, K. (2021). Analyzing block chain adoption barriers in manufacturing supply chains by the neutrosophic analytic hierarchy process. *Annals of Operation Research*, *327,* 129-156. https://doi.org/10.1007/s10479-021-04048-6

Vafadarnikjoo, A., Mishra, N., Govindan, K., & Chalvatzis, K. (2018). Assessment of consumers' motivations to purchase a remanufactured product by applying fuzzy Delphi method and single valued neutrosophic sets. *Journal of Cleaner Production*, *196*, 230–244. https://doi.org/10.1016/j.jclepro.2018.06.037

Vafadarnikjoo, A., & Scherz, M. (2021). A hybrid neutrosophic-grey analytic hierarchy process method: decision-making modelling in uncertain environments. *Mathematical Problems in Engineering*, *2021*, Article 1239505. https://doi.org/10.1155/2021/1239505

Vilasan, R. T., & Kapse, V. S. (2021). Evaluation of the prediction capability of AHP and F_AHP methods in flood susceptibility mapping of Ernakulam District (India). *Natural Hazards, 112,* 1767–1793. https://doi.org/10.21203/rs.3.rs-655658/v1

Wang, H., Smarandache, F., Zhang, Y., & Sunderraman, R. (2010). Single valued neutrosophic sets. *Multispace Multistruct, 4*, 410–413.

Wu, X., Wang, H. J., Saito, Y., Syvitski, J., Bi, N., Yang, Z., Xu, J. P., & Guan, W. (2022). Boosting riverine sediment by artificial flood in the Yellow River and the implication for delta restoration. *Marine Geology*, *448,* Article 106816. https://doi.org/10.1016/j.marg eo.2022.106816

Yang, X. L., Ding, J. H., & Hou, H. (2013). Application of a triangular fuzzy AHP approach for flood risk evaluation and response measures analysis. *Natural Hazards*, *68*(2), 657–674. https://doi.org/10.1007/s11069-013-0642-x

Ye, J. (2017). Single-valued neutrosophic similarity measures based on cotangent function and their application in the faultdiagnosis of steam turbine. *Soft Computing*, *21*, 817–825. https://doi.org/10.1007/s00500-015-1818-y

Yucesan, M., & Gul, M. (2021). Failure prioritization and control using the neutrosophic best and worst method. *Granular Computing, 6*, 435–449. https://doi.org/10.1007/s41066-019-00206-1

Zadeh, L. A. (1965). Fuzzy sets. *Information and Control, 8,* 338–353. https://doi.org/10.1016/S0019-9958(65)90241-X

Zhang, W., Villarini, G., Vecchi, G. A., & Smith, J. A. (2018). Urbanization exacerbated the rainfall and flooding caused by hurricane Harvey in Houston. *Nature, 563*, 384–8. https://doi.org/10.1038/s41586-018-0676-z